



ZIKV can infect human term placentas in the absence of maternal factors

Diana L. Villazana-Kretzer^{1,5}, Kathryn McGuckin Wuertz^{2,5}, Daniel Newhouse², Jennifer R. Damicis³, Elisabeth M. Dornisch³, Kathleen M. Voss², Antonio E. Muruato², Jennifer A. Paymaster¹, Stacey S. Schmiedecke¹, Sarah M. Edwards¹, Peter G. Napolitano⁴, Jennifer Tisoncik-Go², Nicholas Ieronimakis^{1,3,6}  & Michael Gale Jr^{2,6} 

Zika virus infection can result in devastating pregnancy outcomes when it crosses the placental barrier. For human pregnancies, the mechanisms of vertical transmission remain enigmatic. Utilizing a human placenta-cotyledon perfusion model, we examined Zika virus exposure in the absence of maternal factors. To distinguish responses related to viral infection vs. recognition, we evaluated cotyledons perfused with either active or inactivated Zika virus. Active Zika virus exposure resulted in infection, cell death and syncytium injury. Pathology corresponded with transcriptional changes related to inflammation and innate immunity. Inactive Zika virus exposure also led to syncytium injury and related changes in gene expression but not cell death. Our observations reveal pathologies and innate immune responses that are dependent on infection or virus placenta interactions independent of productive infection. Importantly, our findings indicate that Zika virus can infect and compromise placentas in the absence of maternal humoral factors that may be protective.

¹Division of Maternal Fetal Medicine, Madigan Army Medical Center, Tacoma, WA, USA. ²Center for Innate Immunity and Immune Disease, Department of Immunology, University of Washington School of Medicine, Seattle, WA, USA. ³Department of Clinical Investigation, Madigan Army Medical Center, Tacoma, WA, USA. ⁴Department of OB/GYN, University of Washington Medical Center, Seattle, WA, USA. ⁵These authors contributed equally: Diana L. Villazana-Kretzer, Kathryn McGuckin Wuertz. ⁶These authors jointly supervised: Nicholas Ieronimakis, Michael Gale Jr.
✉email: nicholas.m.ieronimakis.civ@mail.mil; mgale@uw.edu

Zika virus (ZIKV) is a flavivirus primarily transmitted by *Aedes* mosquitoes and sexual contact^{1–3}. ZIKV infection during pregnancy has been associated with severe adverse outcomes including microcephaly, intracranial calcification, growth restriction, optical nerve damage, and fetal demise^{4,5}. Pathology accompanies the presence of ZIKV in human amniotic fluid, fetal brain, and placenta^{6,7}. The mechanisms of ZIKV infection and vertical transmission are complex and appear dependent on multiple variables⁸.

Evidence from animal and cell culture models suggest that ZIKV passes to the fetus by infecting the extraembryonic trophoblast and the placenta later in gestation^{9–12}. Experimental models have also revealed several molecular mechanisms related to placental infection and injury¹³. Translating these findings is challenging due to the unique characteristics of the human placenta¹⁴. Human placenta samples are also generally acquired following delivery, well past the phases of infection and fetal injury. The inaccessibility of human placenta samples during acute phases of infection makes vertical transmission difficult to understand and corroborate with experimental findings. Consequently, postpartum placental samples may not reflect the initial mechanisms of placental cell invasion and replication; elements critical for understanding and preventing vertical transmission.

The heterogeneity of ZIKV associated outcomes confounds the underpinnings of placental infection. Around 1 in 10 pregnancies confirmed positive for ZIKV develop noticeable birth defects^{15,16}. The risk and severity of complication decreases with the progression of pregnancy¹⁷. However, almost half of ZIKV infections are asymptomatic and therefore the extent of afflicted pregnancies remains debated¹⁸. ZIKV infection can also persist in placentas to term even when no longer detectable in maternal blood and in cases that tested negative^{19,20}. Such irregularities in symptoms and outcomes suggest that vertical transmission is not only contingent on the timing of infection but more importantly individual factors. Maternal humoral responses appear to influence adverse pregnancy outcomes related to ZIKV infection²¹. However, the impact of maternal factors on human susceptibility to vertical transmission are not readily distinguishable from intrinsic placental responses.

While maternal humoral factors can influence ZIKV pathogenesis in human placentas, intrinsic responses may explain why a large proportion of infected pregnancies are absent fetal complications. We hypothesize that human placentas respond to ZIKV infection independently of maternal influence and that specific responses might link with pathology. To determine placental-specific responses to viral infection, we examined ZIKV exposure in the absence of maternal factors utilizing a human dual-cotyledon, dual-perfusion model^{22,23}. This platform represents a living system with intact maternal-fetal barrier, immune system, and functional vasculature^{22,23}. Importantly, two cotyledons from the same human placenta are compared simultaneously. Other key elements of this assay include the removal of maternal blood (and related factors) and the monitoring of placental function during ZIKV exposure.

We compared active and ultraviolet light (UV)-inactivated ZIKV (iZIKV) to gain insight on immune and infection-related responses associated with viral replication. To distinguish specific responses to ZIKV and iZIKV, virus exposed cotyledons were perfused in parallel to unexposed cotyledons from the same placentas. Term placentas delivered by cesarean from uncomplicated pregnancies were used to avoid confounders and labor-related changes²⁴. Term placentas are prophetically less susceptible to ZIKV infection as compared to earlier in gestation²⁵. We postulated that a lack of infection is indicative of intrinsic mechanism related to placental maturity. Conversely, the presence of ZIKV infection and injury would suggest that human placentas are vulnerable absent maternal humoral factors that may facilitate resistance *in vivo*.

Results

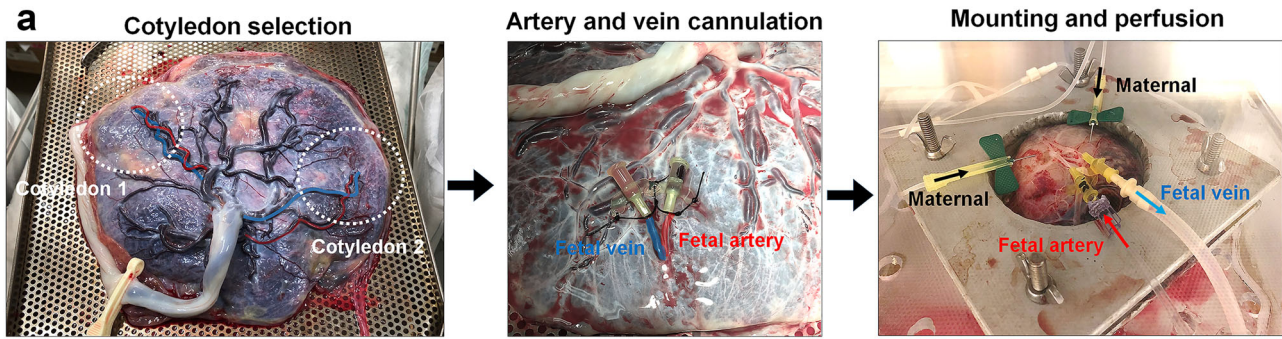
ZIKV exposure invokes subtle physiological and metabolic changes. We blindly collected placentas from uncomplicated cesarean deliveries for exposure to ZIKV or iZIKV in our dual-cotyledon, dual-perfusion system. Placentas utilized for ZIKV and iZIKV perfusions (Fig. 1a, b) show similar characteristics, with two exceptions (Supplementary Data 1). Inadvertently, there is a significant difference between maternal race and fetal sex between placentas utilized for ZIKV vs. iZIKV perfusion experiments. The majority of iZIKV-perfused placentas are from deliveries with female offspring, whereas ZIKV-perfused placentas are mostly from Caucasian mothers. Other characteristics, such as Body Mass Index (BMI), gestational age, and birth weight, are not significantly different between groups.

Physiological monitoring of fetal artery pressures show perfusion with ZIKV slightly but significantly reduces vascular tone at 22 h as compared to control-perfused cotyledons from the same placentas (Fig. 1c). Changes in arterial pressure are not observed in cotyledons perfused with iZIKV relative to the control-perfused cotyledons. Metabolic analysis of the venous effluents collected at the end of each experiment show no difference between control and ZIKV-perfused cotyledons (Supplementary Information). Importantly, lactate values being low and similar among groups indicates that cotyledons were metabolically viable²⁶. The only observed change is the partial pressure of oxygen (PO₂) for virus exposed and control cotyledons as compared to PO₂ levels of the media prior to arterial perfusion. This may relate to oxygen consumption and dilution as the buffer passes through the cotyledons vasculature.

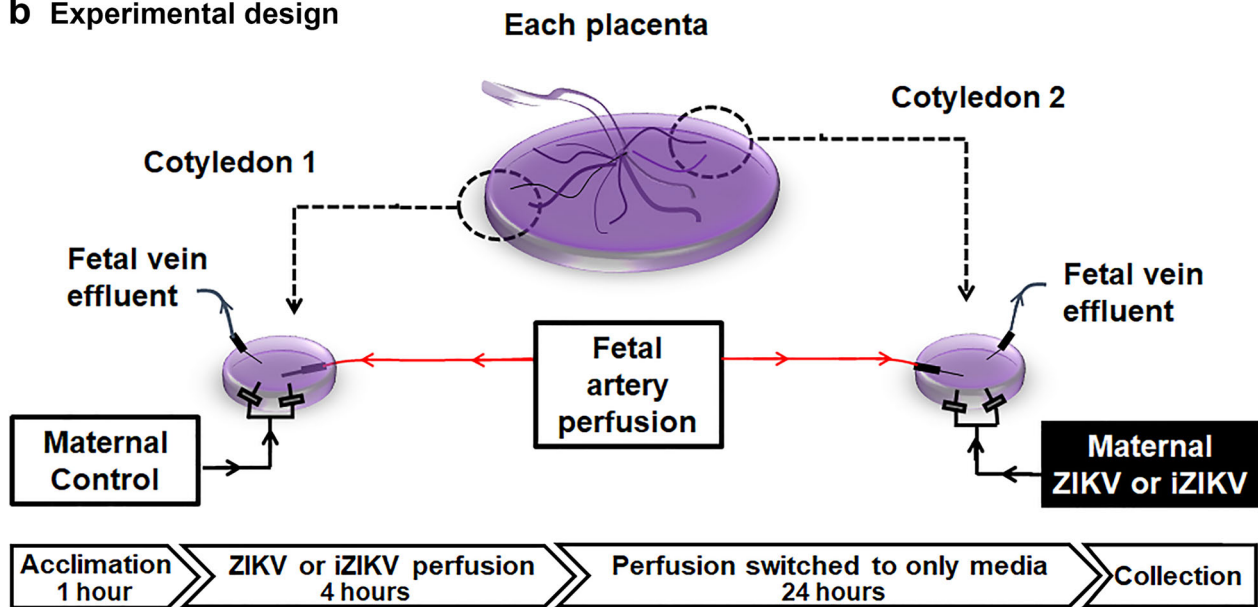
ZIKV infection in perfused human cotyledons. Taking into account that iZIKV lacked infection potential by plaque assay (Fig. 2a), the presence of viral RNA was only measured in ZIKV exposed samples. Postperfusion quantitative real-time PCR (qRT-PCR) analysis of three biopsies per ZIKV exposed cotyledon reveals the presence of viral RNA (Fig. 2b). The viral RNA copy numbers are highly variable and not significantly different ($p > 0.05$ by one-way ANOVA) between biopsies or cotyledons. Immunohistochemistry for NS1 corroborates the presence of ZIKV in exposed cotyledons (Fig. 2c). NS1 was absent in both control and baseline samples, suggesting the antibody is specific (Fig. 2d). The IgG isotype control validates the lack of non-specific binding in these samples (Fig. 2c). Confocal microscopy reveals colocalization of ZIKV NS1 with Cytokeratin 7 and CD163, markers of placental trophoblasts and Hofbauer cells, respectively (Fig. 3a, b)^{27,28}. NS1+/Cytokeratin 7+ and NS1+/CD163– cells were restricted to the syncytium whereas all NS1+/CD163+ cells were within the villous stroma. Once more sections from control-perfused samples (Fig. 3c, d) and ZIKV exposed samples given the IgG isotypes in lieu of the primary antibodies (Fig. 3e) lacked positive staining. Analogous to these results no positive staining is observed in iZIKV perfused samples and their respective controls (Fig. 4).

Syncytium injury and cell death result from ZIKV exposure. Histopathology analysis of perfused tissue reveals damage to the placental barrier with ZIKV (Fig. 5a) and iZIKV (Fig. 5b). The injury represents PLAP+ membrane particles (aka exosomes or blebs) shedding into the intervillous space from the syncytium²⁹. The presence of syncytium injury is significantly greater with ZIKV and iZIKV exposure compared to controls and ase-line samples (Fig. 5c), suggesting that cellular damage occurs irrespective of the virus status.

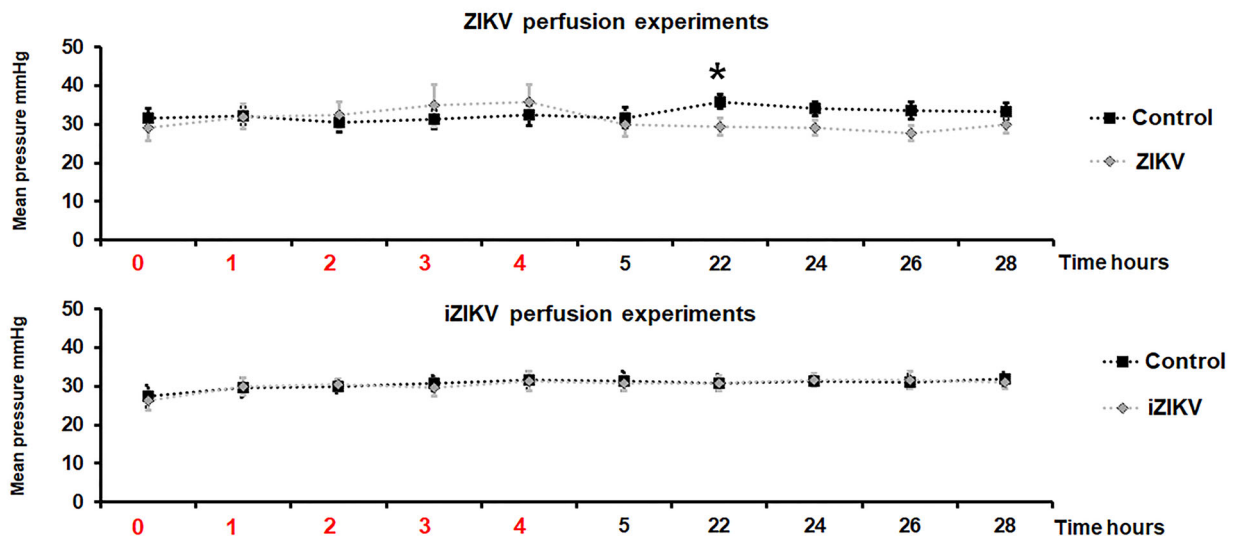
To evaluate if placental barrier injury corresponds with changes in key cellular processes, we quantified indicators of cell death (TUNEL), cell division (Ki67), and cellular-mediated



b Experimental design



c Arterial vascular resistance



inflammation (CD163) from all perfusion experiments. CD163 is present on Hofbauer cells and released in soluble form with inflammation³⁰. Thus CD163 staining may reflect placental Hofbauer cell numbers and their status. With ZIKV, more regions containing TUNEL+ nuclei are visible (Fig. 6a)^{31,32}. A significant increase of TUNEL+ cells occurs with ZIKV exposure

(Fig. 6b). Samples exposed to iZIKV are not significantly different versus controls, but there is a difference in comparison to baseline samples. There is no such pattern with Ki67+ nuclei marking proliferating cells (Fig. 7) or CD163+ cells (Fig. 8) between no differences are observed with Ki67 or CD163 staining's between perfusion conditions (Figs. 7b and 8b).

Fig. 1 Experimental configuration and design. **a** Representation of cotyledon selection, cannulation, mounting, and the configuration for perfusing fetal vessels and the intervillous space. Arrows indicate direction of flow. Blue denotes the main cotyledon fetal vein, red the fetal artery, and black the intervillous space (maternal side). **b** Experimental design for the dual-cotyledon, dual-perfusion assay. Active ZIKV or UV-inactivated ZIKV (iZIKV) virus was infused into the maternal side of experimental cotyledons. In parallel, control cotyledons isolated from the same placentas are infused with media only. Media perfused into the fetal circuit through arterioles (red arrows), effluxes from fetal veins (blue arrows). Following 4 h of viral exposure, cotyledons were perfused with media only for an additional 24 h before biopsy collection. **c** The mean arterial pressures (mmHg) recorded over time for ZIKV ($n = 10$) vs. iZIKV ($n = 9$) perfusion experiments. Red numbers along the x-axis indicate the timeframe of viral exposure for ZIKV and iZIKV infused cotyledons. * denotes $p < 0.05$ by unpaired student's t -test and error bars represent the standard error of the mean.

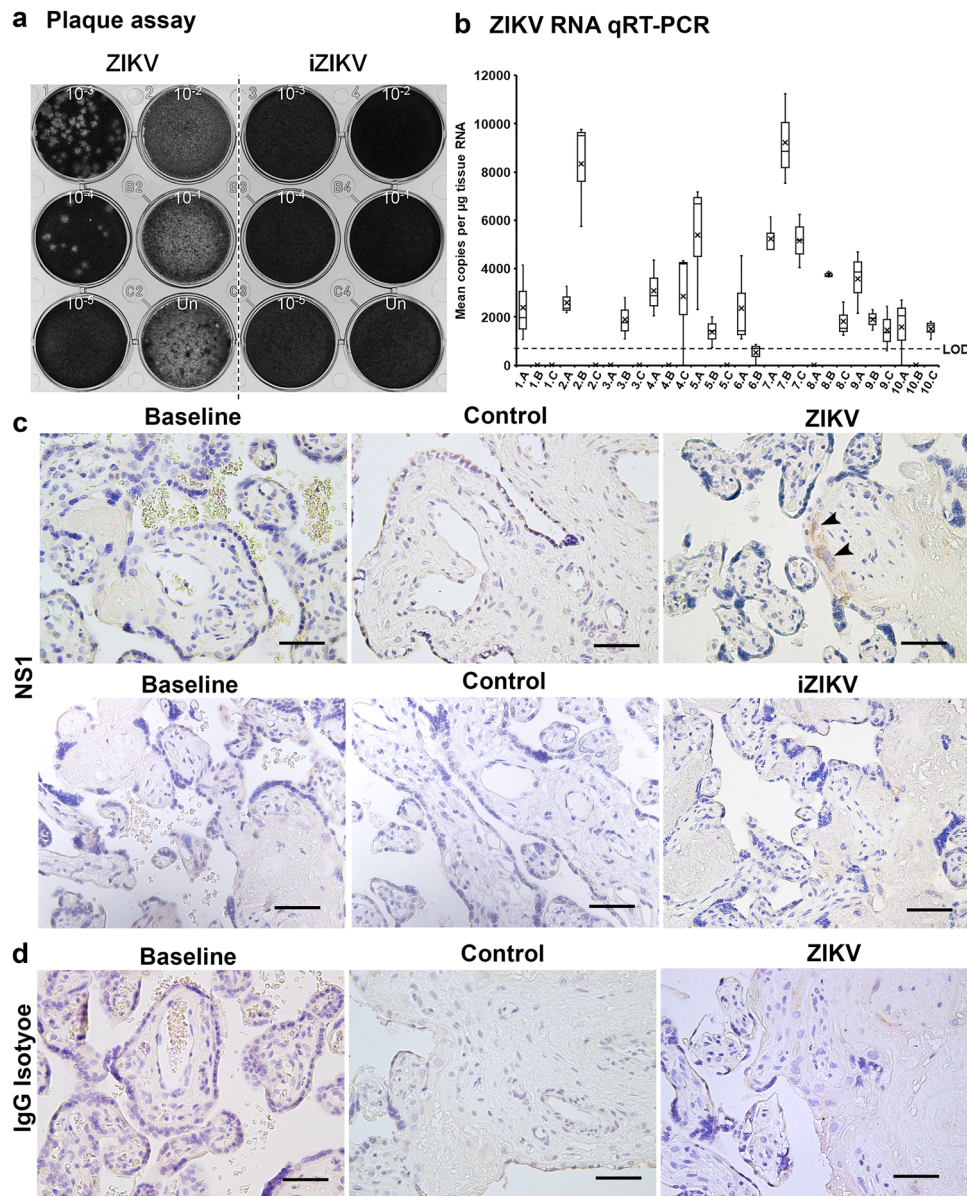


Fig. 2 ZIKV infection in perfused cotyledons. **a** Plaque assay validation of viral stocks depicted in grayscale. Vero cells were inoculated with 100 μ l of Undiluted (Un) and as annotated 10-fold serial dilutions of ZIKV and iZIKV in parallel. **b** Quantitative real-time PCR (qRT-PCR) analysis for ZIKV RNA. A-C represent the three biopsies collected and analyzed from each ZIKV perfused cotyledon (1-10). Box-plots represent the median in the centerline, upper and lower quartiles at top and bottom of box, min/max points as whiskers and the mean as x. LOD represents the limit of detection. **c** Staining for ZIKV NS1 in samples collected at baseline and following perfusion. NS1 staining is visualized with DAB in brown (arrowheads). **d** Staining's conducted in parallel using an IgG isotype in place of NS1. Hematoxylin was used to counterstain nuclei in blue. Scale bars = 50 μ m.

ZIKV infection and pathology correspond with unique transcriptional changes. To understand the mechanisms of ZIKV infection and pathology, we used the NanoString nCounter gene expression assay to investigate immune-related and adhesion

molecule gene signatures. The NanoString Human PanCancer Immunology Panel has been used for the immunologic characterization of peripheral blood of ZIKV-infected patients³³. Differential expression (DE) analysis of each virus perfusion was

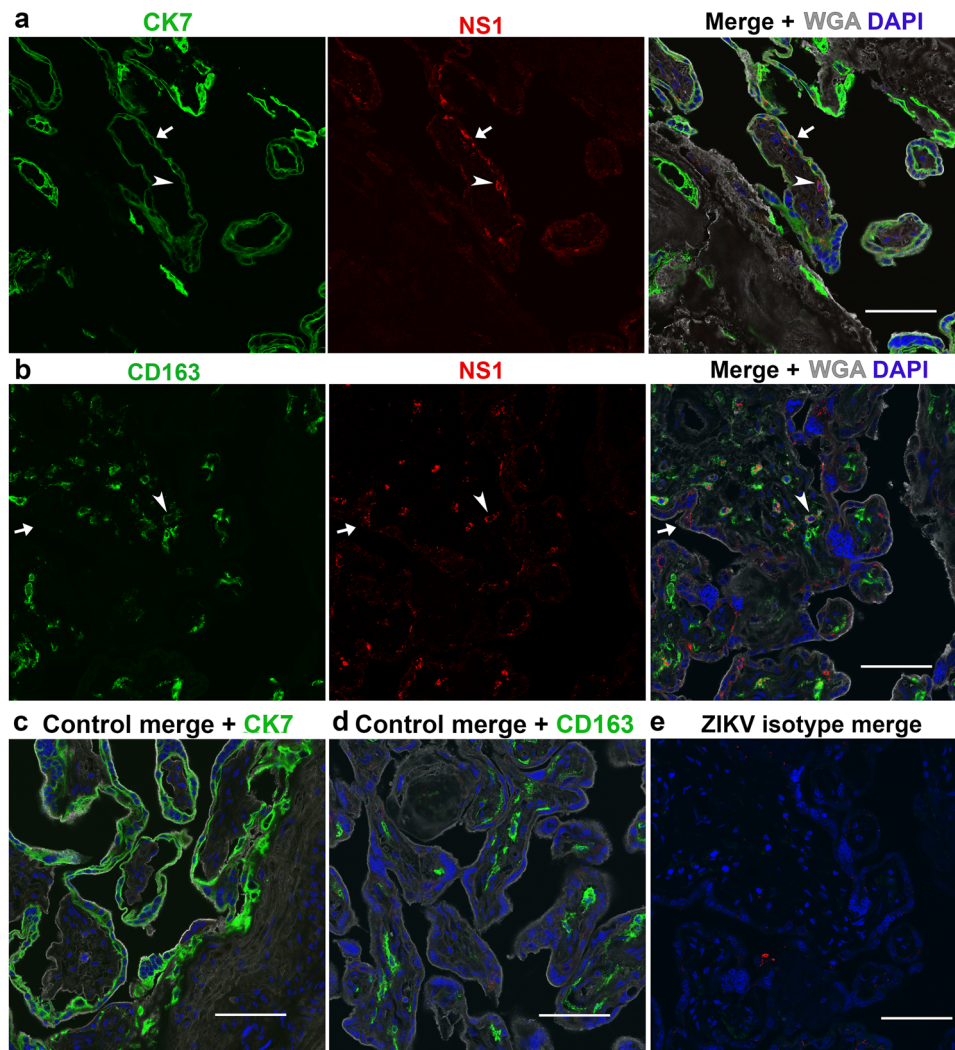


Fig. 3 NS1 colocalization in ZIKV perfused cotyledons. a–b Confocal images acquired from cotyledons exposed to ZIKV. Sections were stained with Cytokeratin 7 (CK7) or CD163 depicted in green, along with NS1 in red, the lectin WGA in gray and DAPI as blue. Arrows denote colocalization of NS1 with CK7 or CD163 positive cells, respectively. Arrowheads denote NS1 staining that does not colocalize. **c–d** Merged images of NS1, WGA, DAPI, and CK7 or CD163 staining's in control cotyledons perfused in parallel to ZIKV. **e** Representative image of serial sections from ZIKV exposed sample stained with IgG isotype antibodies in place of anti-CK7, CD163 and NS1. Scale bars = 50 μ m.

compared to respective control cotyledons. We also investigated DE genes by direct comparison of ZIKV and iZIKV perfusions³³. With few exceptions, the most prominent DE expressed genes do not overlap between ZIKV vs. control as compared to iZIKV vs. control (Fig. 9a and b). Mainly chemokine *C-C Motif Chemokine Ligand 18 (CCL18)*, *Transforming Growth Factor Beta 2 (TGFB2)* and *Thrombospondin 1 (THBS1)* were related to ZIKV and iZIKV when compared to their respective controls (Fig. 9b). The pattern of expression (upregulation vs. downregulation) contrasts between samples infected with ZIKV as compared to those exposed to iZIKV (Fig. 9b and c). Among these genes, *AXL Receptor Tyrosine Kinase (AXL)* and *Toll-Like Receptors (TLRs)* have been implicated for ZIKV infection^{34–36}. With ZIKV infection, several genes related to innate immunity and Hofbauer cells are reduced or downregulated in expression compared to controls. Notably *C-X-C Motif Chemokine Ligand 6 (CXCL6)*, *Interleukin 6 Receptor (IL6R)*, and *Interleukin 24 (IL24)* are lower with ZIKV infection^{37–39}. Genes increased or upregulated in expression include key regulators of immune responses, *PDCD1* and *TLR5*^{40,41}. A complete list of significant DE genes is provided in the Supplementary Data 2 file.

In spite of these differences, we did not observe changes in interferon-stimulating genes (ISG) as anticipated with ZIKV exposure⁴². Therefore, we examined the expression for an indicator of interferon responses, *Interferon Induced Transmembrane Protein 1 (IFITM1)* by qRT-PCR. The expression of *IFITM1* was lower between controls and ZIKV or iZIKV exposed samples but this was not significant (Fig. 9d). Being that interferons do not appear robustly activated, we conducted canonical pathway analysis using IPA to understand the immune and inflammatory processes related to the observed transcriptional patterns (Fig. 9). To distinguish differences between infection and exposure, this analysis was conducted for ZIKV and iZIKV vs. their respective controls. With ZIKV, most of the top-ranking pathways are activated and include the Role of Pattern Recognition Receptors in Recognition of Bacteria and Viruses, Triggering Receptor Expressed on Myeloid cells 1 (TREM1) Signaling, and the T helper type-2 (Th2) Pathway (Fig. 10a). A greater number of pathways are inactivated with iZIKV, notably Natural Killer Cell Signaling, which is activated by ZIKV (Fig. 10a). Th1 and Th2 pathways were also inactivated with iZIKV but active with ZIKV. In contrast, the Neuroinflammation

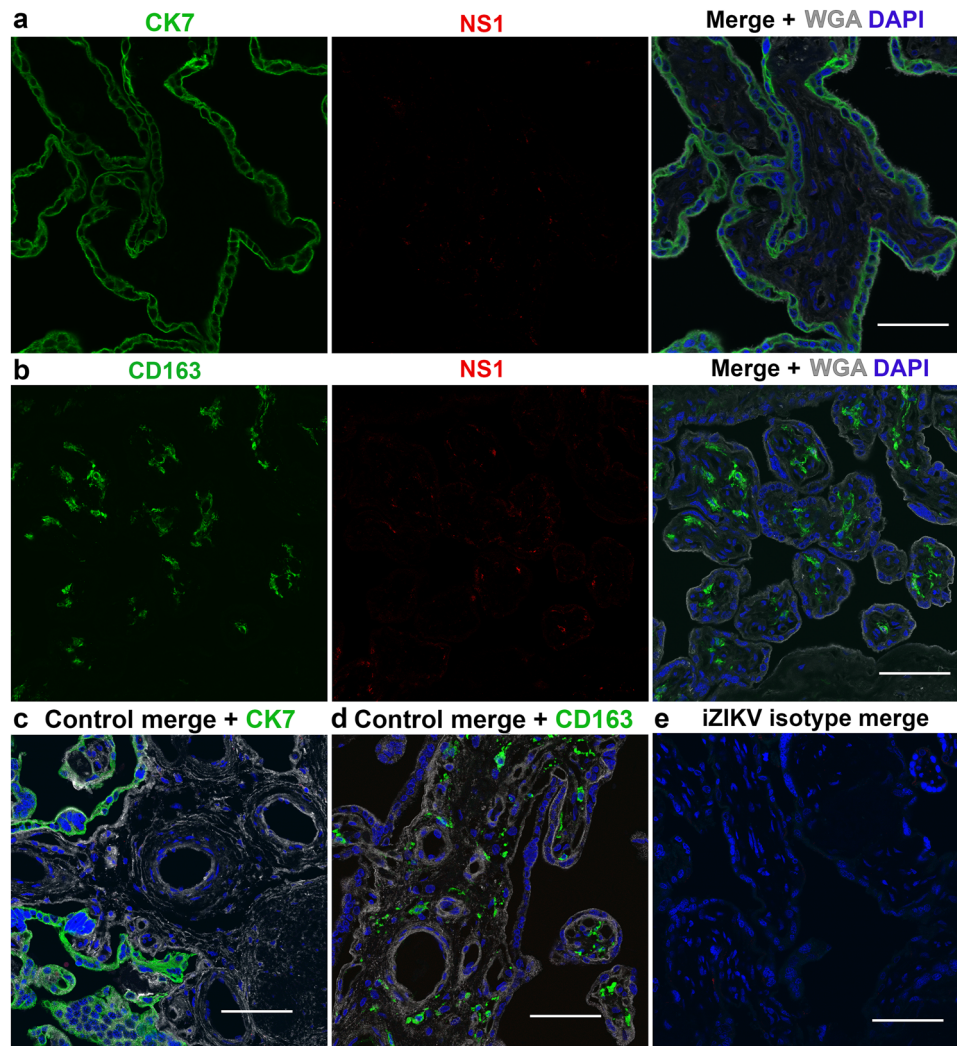


Fig. 4 Absence of NS1 in iZIKV perfused cotyledons. **a–b** Confocal images acquired from cotyledons exposed to iZIKV. Parallel to Fig. 4 sections were stained with Cytokeratin 7 (CK7) or CD163 depicted in green, along with NS1 in red, the lectin WGA in gray and DAPI as blue. **c–d** Merged images of NS1, WGA, DAPI, and CK7 or CD163 staining's in control cotyledons perfused in parallel to iZIKV. **e** Representative image of serial sections from iZIKV exposed samples stained with IgG isotype antibodies in place of anti-CK7, CD163 and NS1. Scale bars = 50 μ m.

Signaling Pathway was inactive with ZIKV but active with iZIKV. Only the Role of Pattern Recognition Receptors in Recognition of Bacteria and Viruses and Hepatic Fibrosis Signaling Pathways were similar in activation status between ZIKV and iZIKV. The remaining relationships were group specific. Notable inflammatory pathways activated with ZIKV include Toll-like Receptor, IL-8 Signaling and Production of Nitric Oxide and Reactive Oxygen Species in Macrophages. In contrast, STAT3, IL-2, IL3, and IL-17 Signaling were activated with iZIKV.

Discussion

Maternal symptoms related to ZIKV infection are heterogeneous or often absent⁴³. There is no association between maternal health status and fetal complications related to ZIKV⁴⁴. However, inflammatory factors are elevated in maternal blood in pregnancies complicated by ZIKV⁴⁵. Humoral factors may not associate with human maternal health, but they appear to influence adverse pregnancy outcomes associated with congenital ZIKV syndrome (CZS)²¹. Evidence from animal models suggests this to be the case⁴⁶. Yet, the influence of maternal factors on human placental immunity is not easily distinguishable from intrinsic responses.

Our study demonstrates that ZIKV can infect human term placentas in the absence of maternal factors. Signs of infection and pathology were present in all cotyledons exposed to the active ZIKV. These results suggest that maternal humoral factors may be protective, particularly since fetuses in the third trimester and by extension their placentas, are believed to be less susceptible¹⁷. The ability of ZIKV to infect and damage perfused term human cotyledons, in an experimental model free of maternal influence supports this possibility. This notion coincides with the observation that the majority of ZIKV infected pregnancies are absent complications. In our experiments, ZIKV exposed cotyledons were afflicted in a virus-specific manner. However, the threshold for placenta injury, including cell death and syncytium injury, in relation to ZIKV transmission remains unknown.

Crosstalk between maternal and fetal responses to ZIKV may govern placenta immunity and vertical transmission. Irregularities of ZIKV related outcomes in dizygotic twins suggest that individual fetal components are involved⁴⁷. The placenta is fetal-derived tissue and may react differently to ZIKV and maternal factors depending on genetic and epigenetic factors. Though we did observe infection and injury in all placentas exposed to ZIKV, the observed variability may relate to individual genetic or clinical

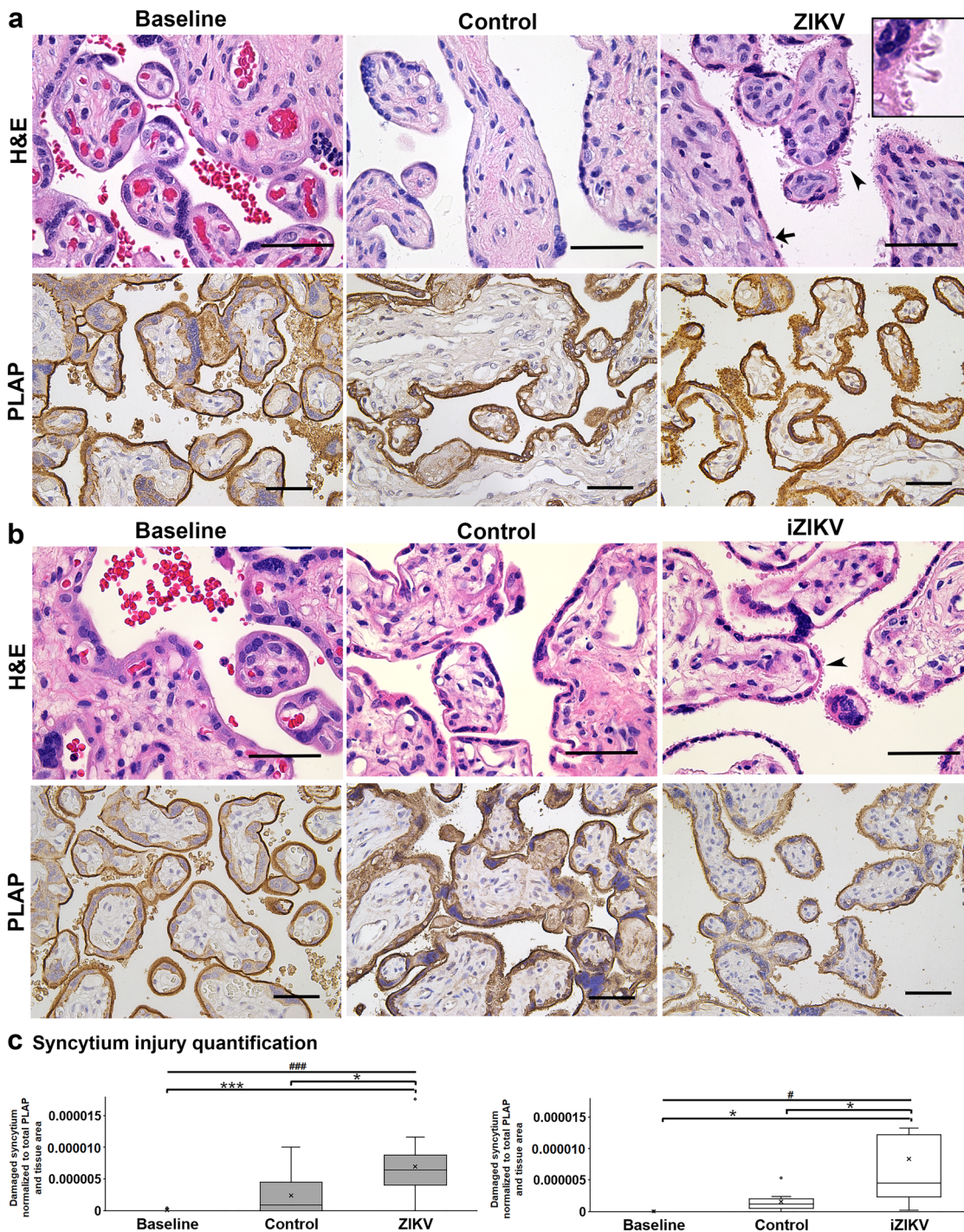


Fig. 5 ZIKV and iZIKV invoke syncytium injury. H&E and PLAP staining representing syncytium remodeling (arrowheads) at Baseline and following exposure to ZIKV (a) and iZIKV (b). In the ZIKV panel, an arrow denotes normal syncytium and the inset (right corner) magnifies the damaged region designated by the arrowhead. PLAP staining is represented by DAB in brown. Scale bars = 50 μ m. **c** Quantification of syncytium remodeling in PLAP stained sections normalized to the total area of tissue within each image analyzed. The left graph represents $n = 10$ and right graph $n = 9$ samples per condition. Box-plots represent the median in the center line, upper and lower quartiles at top and bottom of box, min/max points as whiskers, outliers as dot, and the mean with x . # $p < 0.005$, ### $p < 0.0005$ by one-way ANOVA. * $p < 0.05$, *** $p < 0.0005$ by Tukey's post-hoc test.

characteristics. Therefore, certain fetal and maternal predispositions may coalesce to enable ZIKV transmission.

During pregnancy the placenta develops predominately innate immune components whereas adaptive immunity is mainly maternal¹². Fetal-maternal symbiosis involves declines in adaptive immune cells and function⁴⁸. This process enables fetal tolerance at the cost of increased maternal vulnerability to

infection⁴⁹. Incidentally, maternal humoral factors are important component of fetal protection that can also lead to complications. Specifically, immunoglobulin G (IgG) antibodies cross the placenta early in pregnancy to provide passive immunity but can also invoke fetal autoimmune disorders^{50,51}. Within the context of ZIKV, evidence suggests that transplacental IgGs enhance fetal infection and promote adverse outcomes²¹. However, this may

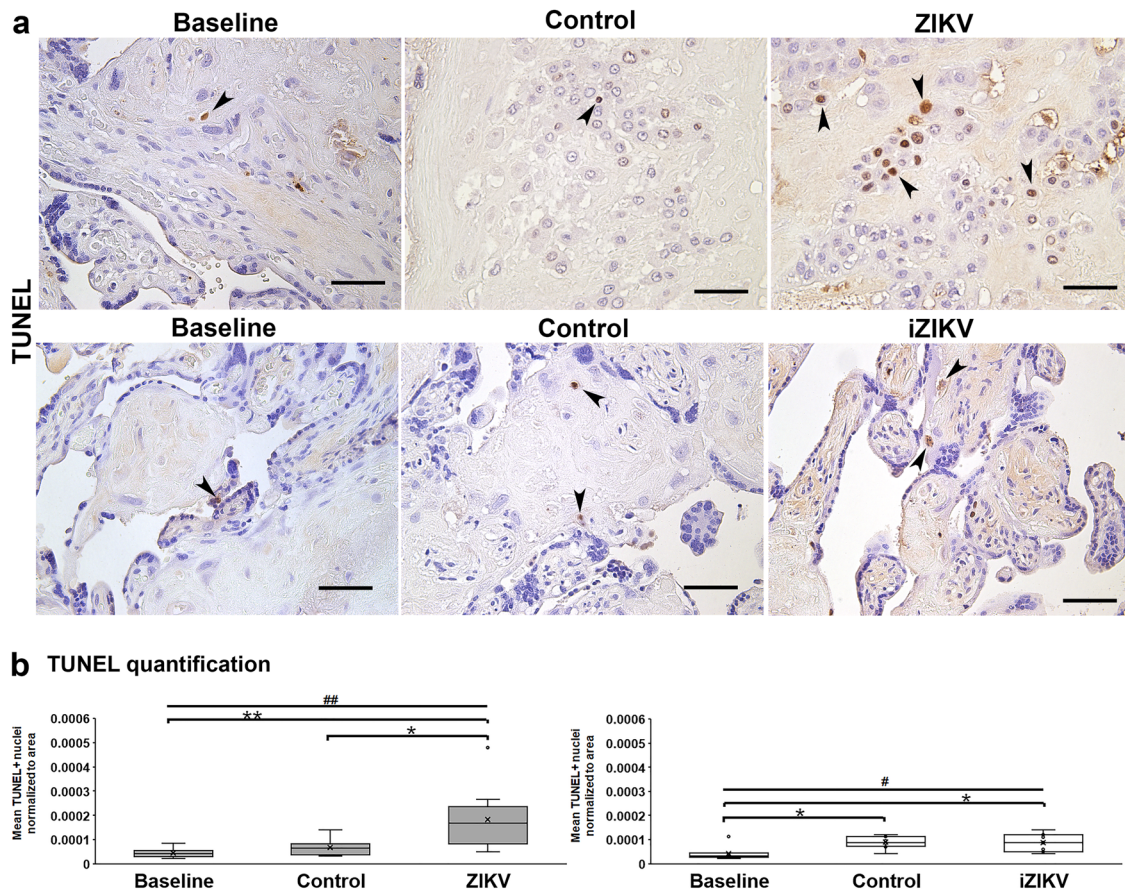


Fig. 6 Cell death elevated with ZIKV perfusion. a Representative TUNEL staining with DAB in Baseline, Control, ZIKV, and iZIKV exposed samples. TUNEL positive cells (arrowheads) appear as brown nuclei vs. blue nuclei counterstained with hematoxylin. Scale bars = 50 μ m. **b** Quantification of TUNEL positive nuclei normalized to the area of tissue within each field analyzed. The left graph represents $n = 10$ and right graph $n = 9$ samples per condition. Box-plots represent the median in the centerline, upper and lower quartiles at top and bottom of box, min/max points as whiskers, outliers as dot, and the mean with x. $\#p < 0.005$, $\#\#p < 0.005$ by one-way ANOVA. $*p < 0.05$, $**p < 0.005$ by Tukey's post hoc test.

depend on the timing of infection; being permissive earlier in gestation and perhaps protective as the placenta and its innate immune system matures.

In conjunction with maternal humoral factors, the fetus relies on the placental barrier and its innate immune defenses for preventing vertical transmission of pathogens. Studies have implicated placental innate immune regulation as a factor in placental susceptibility to ZIKV infection^{52–54}. Our experimental evidence suggests that within intact cotyledons, human placenta cells are susceptible to ZIKV (Figs. 2 and 3). This coincides with cell death and the downregulation of specific innate immune genes that may alter placental function and viral resistance (Figs. 6 and 9)¹⁰. In contrast, syncytiotrophoblast injury occurred with both active and inactive ZIKV exposure (Fig. 5), suggesting that viral products can elicit placenta barrier compromise, independent of infection⁵⁵. This event may enable access to intervillous cells including Hofbauer cells that are vulnerable to ZIKV infection^{25,53,56}.

Hallmarks of ZIKV infection associated with Hofbauer cell infection are signatures of innate immune and antiviral responses⁵⁷. Innate immune activation takes place following ZIKV infection. This process includes the acute virus-induced expression of a variety of antiviral and immune-modulatory genes. Activation is succeeded by the production of types I and III interferons and their induced expression of ISGs⁵⁸. While our gene expression analyses identified innate immune and inflammatory gene regulation following brief exposure or early infection

by ZIKV, we did not identify robust ISG activation in our model. Variations in experimental design and our use of perfused tissue vs. cultured cells may account for this outcome. Additionally, the aforementioned studies observed ISG expression beyond 24 h of ZIKV exposure. It is likely that the differential expression of the immune and inflammatory genes shown here precedes ISG activation in the context of placental ZIKV exposure or infection. This coincides with the lack of cell division or increase of Hofbauer cells (Figs. 7–8) that are observed in vivo and may relate to ISG activation and/or maternal stimuli⁵⁹.

In our comparison, it is possible that the few mutually expressed genes between active and inactive ZIKV exposure support syncytium injury. Alternatively, syncytium injury can occur by different mechanisms initiated by either infection or host interactions. Tissue damage is observed in ZIKV infected placentas and experimental animal models have linked this pathology to type I interferon signaling^{60–62}. Pregnancy complications such as growth restriction arise with ZIKV infection and accompany placental damage^{63,64}. Syncytium injury also manifests in pregnancies complicated by preeclampsia or growth restriction with no known infections⁶⁵. In placentas with ZIKV infection or unrelated pregnancy complications, syncytium injury is accompanied by the activation of inflammatory pathways such as TLR and TNF^{66–68}. Therefore, syncytium injury may be a consequence of inflammation provoked by pathogen exposure or disease. Syncytiotrophoblast molecular pattern sensing likely initiate such destructive inflammatory responses to combat

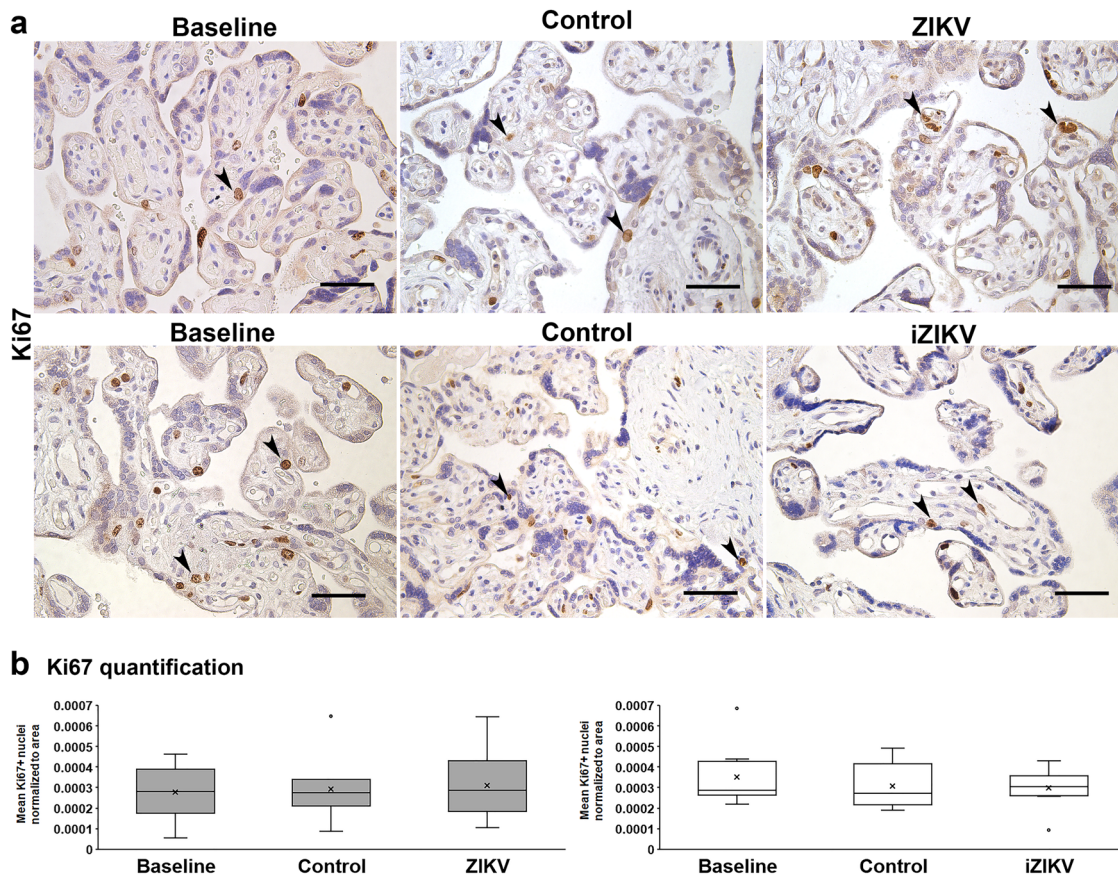


Fig. 7 Cell division unaltered in perfused cotyledons. a Representative of Ki67 staining with DAB and hematoxylin in Baseline, Control, and virus exposed samples. Scale bars = 50 μ m. Ki67 positive cells (arrowheads) appear as brown nuclei vs. blue nuclei counterstained with hematoxylin. **b** Quantification of Ki67 positive nuclei normalized to the area of tissue within each field analyzed. The left graph represents $n = 10$ and right graph $n = 9$ samples per condition. Box-plots represent the median in the centerline, upper and lower quartiles at top and bottom of box, min/max points as whiskers, outliers as dot, and the mean with x.

infection and signal localized and systemic (maternal) defenses. This process may precede the stimulation of placental ISGs, which perhaps activate via a combination of endogenous and circulating factors. Our observations support this possibility as pathogen-related pattern recognition and the activation of several inflammatory pathways accompanied ex vivo syncytium injury (Figs. 5 and 10a).

Taken that not all placental cells are infected yet may react to virus exposure, the responses to ZIKV exposure and infection may not be mutually exclusive. The downregulation of certain genes such as *Interferon Alpha Inducible Protein 27 (IFI27)* with virus exposure supports this possibility as it is upregulated in ZIKV infected human cell cultures⁶⁹. Another possibility is that genes altered by virus exposure are suppressed during ZIKV infection through viral-directed processes⁴². The downregulation of inflammatory genes *CCL18*, *CCL19*, *CXCL6*, *CXCL9*, *IL6R*, *IL11*, *IL24*, and *Integrin Subunit Beta 3 (ITGB3)* with ZIKV infection may reflect placental immune tolerance. (Fig. 9c, Supplementary Data 2). ZIKV infection also resulted in the upregulation of *Programmed cell death protein 1 (PDCD1)*, a gene implicated in immune suppression and cell death⁴⁰. This trend supports the ability of ZIKV to alter immunity and attenuate innate immune programming to facilitate viral replication and spread^{52,57,70}.

Notably, we detected the downregulation of two genes, *Leukemia Inhibitory Factor (LIF)* and *Poliovirus Receptor (PVR)*, related to other viruses yet not currently linked to ZIKV infection. In human placentas, LIF is associated with HIV inhibition⁷¹. In

contrast, *PVR* (aka *CD155*) the canonical poliovirus receptor, is expressed with no known role in the human placenta^{72,73}. Additional investigation and validation are necessary for understanding these patterns of gene expression and conserved mechanisms related to viral infection and pathology in human placentas.

Our transcriptional analysis reveals distinct patterns of expression between ZIKV infection and exposure. Canonical pathways related to the transcription profiles showed little overlap between ZIKV and iZIKV. However, in both cases these pathways reflect innate immunity and inflammatory responses (Fig. 10a). Pathways activated by ZIKV and iZIKV include pattern recognition, which may mediate innate defenses that trigger inflammation and cellular injury. Interestingly, Natural Killer (NK) Cell Signaling was active with ZIKV but inactive with iZIKV. This suggests the virus can be immunosuppressive and that the process of infection provokes inflammatory cell death⁷⁴. With infection, placental cells may also be eliciting maternal reinforcements in the form of NK cells, which are elevated with ZIKV viremia⁷⁵. However, further investigation is warranted to distinguish if such mechanisms combat transmission by signaling maternal inflammation and eliminating infected cells or if they create a permission microenvironment for ZIKV to reach the fetal bloodstream.

Regarding the investigation of ZIKV infection in human placentas, our study has several strengths. Foremost is the use of the human dual-cotyledon, dual-perfusion assay. For examining placental viral infection, this platform offers several advantages: 1. In every perfusion experiment two functional cotyledons from the

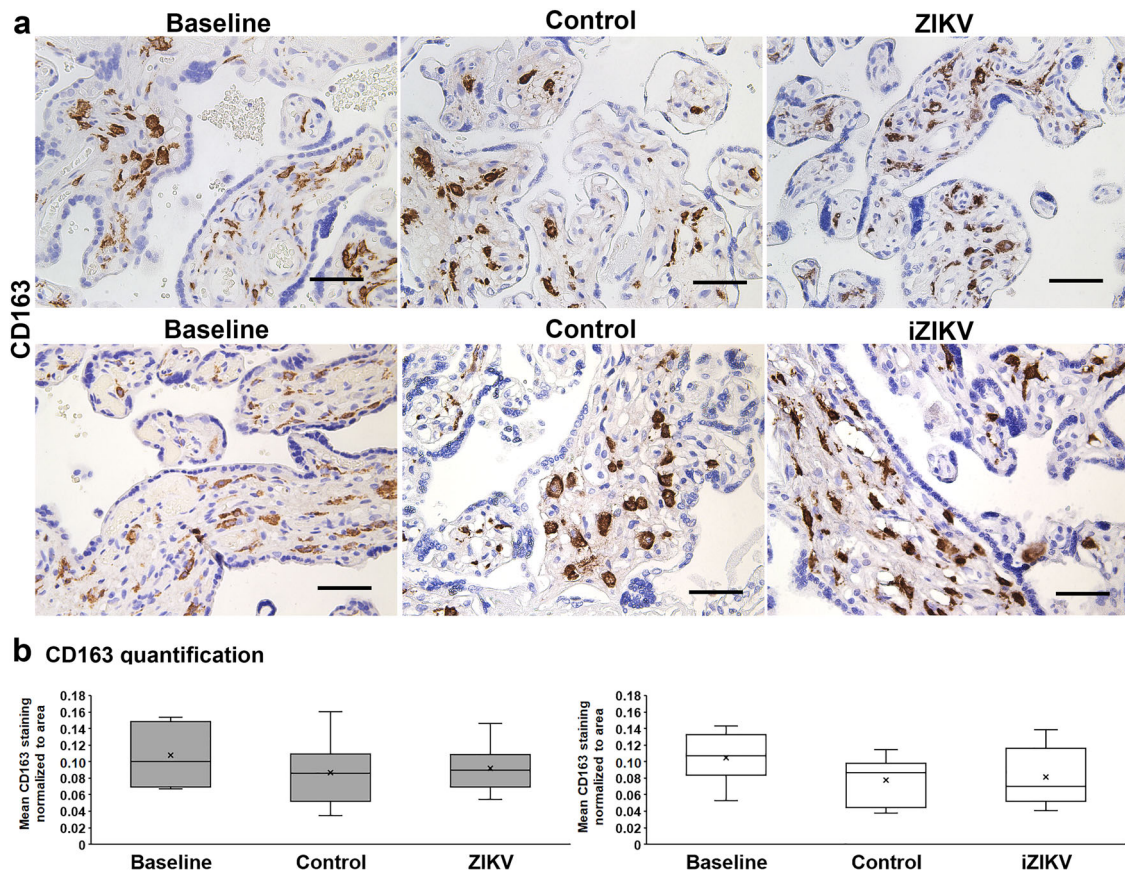


Fig. 8 No change in Hofbauer cells with perfusion. **a** Representative CD163 staining with DAB and hematoxylin in Baseline, Control, and virus exposed samples. Scale bars = 50 μ m. **b** Quantification of CD163 staining normalized to the area of tissue within each field analyzed. The left graph represents $n = 10$ and right graph $n = 9$ samples per condition. Box-plots represent the median in the centerline, upper and lower quartiles at top and bottom of box, min/max points as whiskers, outliers as dot, and the mean with x.

same placenta are run in parallel (control and virus exposed), 2. Simulating in vivo conditions the vasculature and intervillous space are perfused simultaneously, and 3. The absence of circulating humoral factors permits the examination of maternal influence (or rather lack of) on placental infection and injury. Our system is also aseptic, viable, and validated. We optimized our perfusion system to run for over 28 h and confirmed the presence of ZIKV infection by qRT-PCR and immunostaining's. The absence of vasospasm and metabolic changes, specifically in lactate, substantiate the viability of perfused cotyledons²⁶. Finally, the comparison of ZIKV vs. iZIKV enables the distinction of responses related to infection and immunity.

Our study is not without limitations. The first is the predominance of placentas from Caucasian donors with ZIKV perfusions and the fetal sex being mostly female with iZIKV perfusions. This was unintended as experiments are initiated without knowledge of race or fetal sex. In turn, clinicians that consented donors and collected placentas were unaware of the exact virus perfusion treatment. Finally, we received clinical characteristics only when perfusion experiments were successful with placentas free of leakage or damage from the cesarean or processing. We acknowledge differences in clinical characteristics may bias comparisons between active and inactive ZIKV perfusions. However, most comparisons are between cotyledons from the same placentas and likely uninfluenced by such potential confounders.

The main limitation of our study is the use of the term placentas that may not represent events at earlier stages of pregnancy. To date several studies have demonstrated an association between complications and gestational age, providing a link between developmental

maturity and infection^{17,76}. Not all studies correlate adverse outcomes with infection earlier in gestation^{64,77}. Furthermore, the majority of ZIKV infected pregnancies even in the first trimester appear unaffected. Paradoxically, ZIKV infection has been identified in placentas of uncomplicated pregnancies²⁵. Such cases lack placental pathology. In contrast, ZIKV infected pregnancies with adverse fetal outcomes exhibit placental pathology including syncytium injury⁷⁸. Therefore, placental injury is perhaps a determinant of vertical transmission.

The symbiosis between two genetically distinct immune systems (maternal and fetal) is a unique biological process that occurs naturally only in pregnancy. Our understanding of vertical transmission is complicated by the immunological environment of pregnancy; a delicate balance between fetal protection and tolerance. Maternal-fetal interactions may relate to the ability of ZIKV to compromise the placental barrier in some but not all pregnancies. Based on our results we postulate that this may occur via damage to the placental microenvironment when maternal (protective) factors are absent a. In summary, our study further supports the importance of maternal interactions in combating placental infection and viral transmission to the fetus.

Methods

Perfusion experiments. Placenta collections and perfusions were carried out with approval from the Madigan Institutional Review Board. Unlabored placentas were acquired following consent and delivery by cesarean section. Only uncomplicated term pregnancies were included in this study. Pregnancies with complications or with known maternal use of tobacco, drugs or alcohol were excluded. Placentas were processed within 30–60 min of delivery, as previously described^{22,23}. Two cotyledons were excised from individual placentas and the main fetal artery and

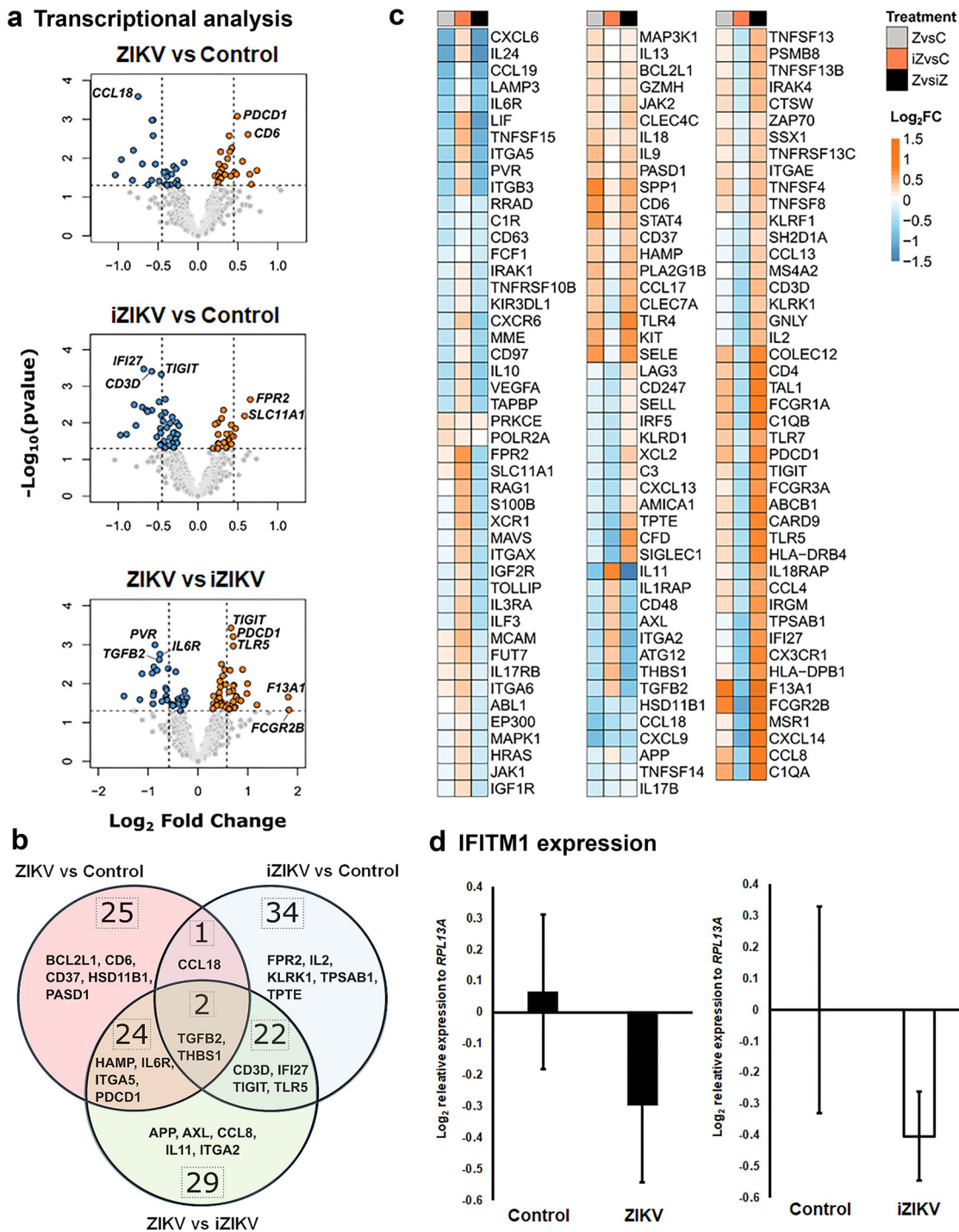
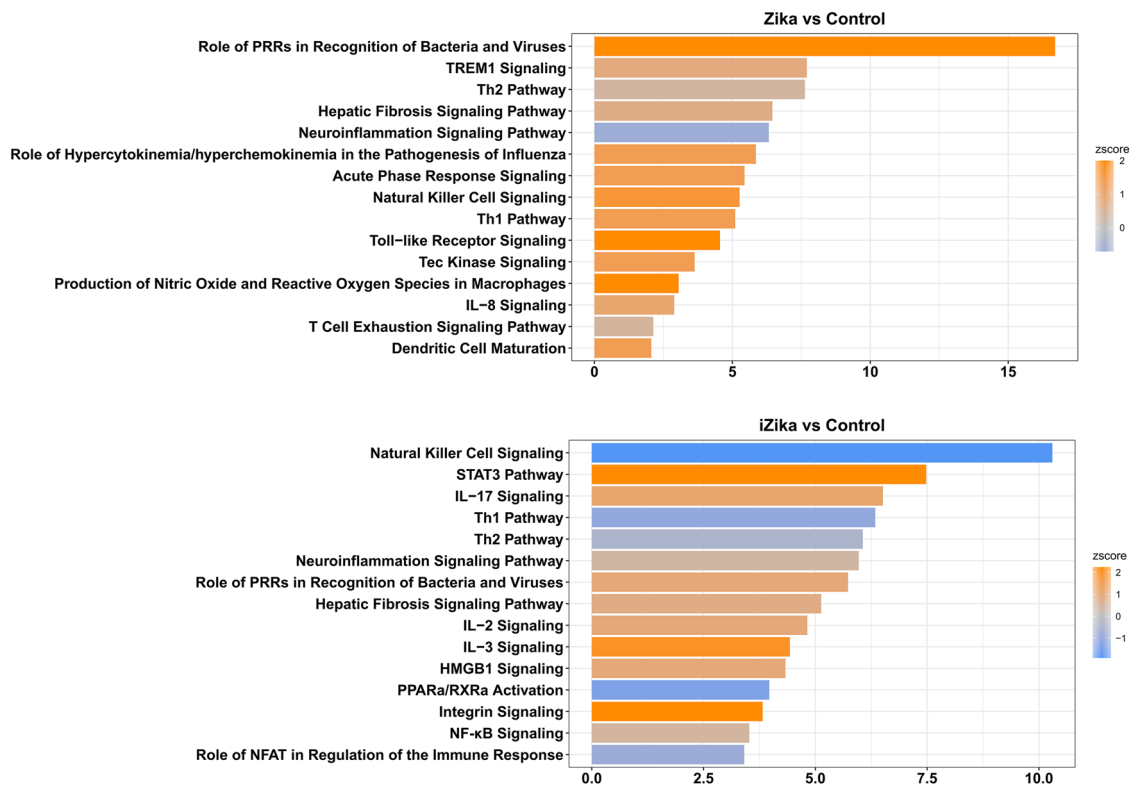


Fig. 9 Transcriptional changes with ZIKV and iZIKV perfusion. a-c nCounter transcriptional analysis in virus perfused vs. Control cotyledons ($n = 5$ samples per condition). **a** Volcano plots of differentially expressed (DE) genes among respective comparisons. Points on the plots represent individual genes. Hashed lines denote a p value < 0.05 , absolute \log_2 fold change > 0.45 for ZIKV and iZIKV vs. Controls, and absolute \log_2 fold change > 0.58 for ZIKV vs. iZIKV wherein the top genes are annotated. Differentially expressed (DE) genes significantly upregulated are shown in red while those downregulated are blue. **(b)** Venn diagram annotating the total number and overlap for significant DE genes between comparisons. The top five most significant genes based on the limma moderated t -statistic are annotated. **c** Heatmaps denoting all significant ($p < 0.05$) DE genes, clustered by complete linkage on Euclidean distances of \log_2 fold change values. **d** The relative expression of *IFITM1* by qRT-PCR in most of the same samples ($n = 5-7$ per condition) examined by the nCounter. Control samples reflect cotyledons from the same placentas used for either ZIKV or iZIKV perfusions respectively. Box-plots represent the median in the centerline, upper and lower quartiles at top and bottom of box, min/max points as whiskers, and the mean with x .

vein were cannulated for perfusion. Two butterfly needles were inserted just below the chorionic plate to simulate maternal perfusion (Fig. 1a). Cotyledons were placed in customized enclosures within an incubator at 36 °C. Cotyledons were continuously perfused with warmed and oxygenated media that was not recirculated, within a laminar hood following BSL2 standards. The media consisted

of Hanks' Balanced Salt solution pH 7.4 (Sigma-Aldrich, St. Louis, MO, USA), containing 2 g/L Albumin (Sigma), 2000 U/L Heparin (Patterson Veterinary Supply, Devens, MA, USA) 5 mg/L Gentamycin, and 0.35 g/L Sodium Bicarbonate (Sigma). The remaining placental tissue was utilized to provide the baseline references. These samples designated as "baseline", constitute fresh unperfused

a Canonical pathway analysis



b Summary of findings

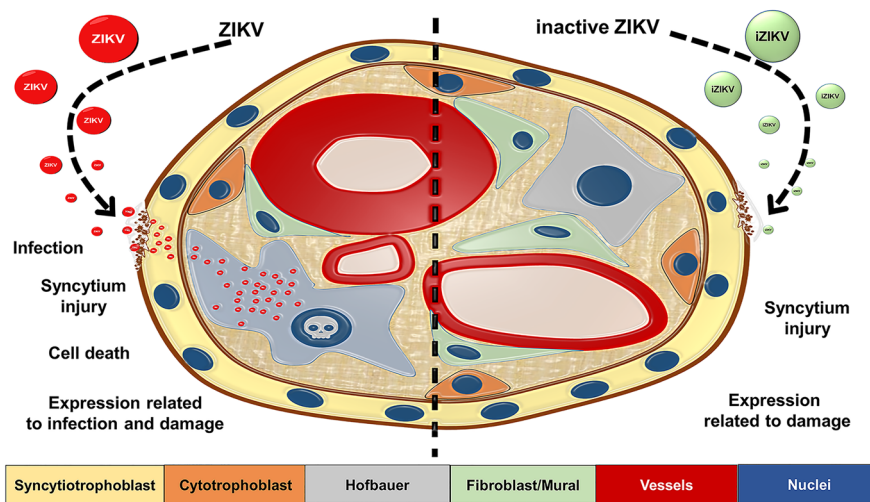


Fig. 10 Network analysis and synopsis. **a** Bar charts of significantly enriched IPA canonical pathways for ZIKV vs. control (top graph) and iZIKV vs. control (bottom graph) DE genesets. Bars represent each canonical pathways *p* value on a negative logarithmic scale. The top 15 pathways related to immunity and inflammation are ranked based on *p* value ≤ 0.05 . Bars are shaded according to their z-score activity predictions. Orange represents pathways with positive z-scores and depicts pathway activation; blue represents pathways with negative z-scores and depicts pathway inactivation. PRRs denote Pattern Recognition Receptors. **b** Summary of findings and potential model of ZIKV transmigration across the maternal-fetal interface.

intervillous biopsies collected as cotyledons designated for perfusion were being prepared.

For the initial acclimation and blood clearance, peristaltic pump rates were 4 mL/minute and 10 mL/minute for fetal and maternal sides, respectively, within the first hour of perfusion^{22,23}. To make volumes manageable for long-term perfusion, rates were adjusted to 1.6 mL/minute (fetal) and 3.3 mL/minute (maternal) for the remainder of each experiment. Viral exposure was initiated after all blood was visibly cleared, indicated by the blanching of cotyledons and clear effluent leaving the venous lines. Cotyledons were randomized to receive via the intervillous space, the vehicle control, or either ZIKV or iZIKV (Fig. 1b). The

iZIKV was derived from the same ZIKV stock (strain Brazil Fortaleza 2015⁵⁸) by exposing the viral stock to ultraviolet (UV) light using a UV-crosslinker for 30 min. Both ZIKV and iZIKV preparations were validated by plaque assay to confirm infectious titer and lack thereof, respectively. Vehicle control cotyledons referred to as “controls”, were perfused in parallel to experimental cotyledons with the same buffer that lacked the addition of either ZIKV or iZIKV. ZIKV or iZIKV was infused into the intervillous space of experimental cotyledons at a dose of 200 plaque-forming units per mL for 4 h then switched to media for an additional 24 h (Fig. 1c). Clinical characteristics for each placenta/donor were received at the conclusion of each successful perfusion experiments (Supplementary Data 1).

Arterial resistance was monitored by inline transducers to validate perfusions and cotyledon viability during the course of each experiment. At the end of each experiment, venous perfusates and baseline media (unperfused buffer), were collected for metabolic analysis (Supplementary Table 1) with the i-STAT CG4+ system/cartridges (Abbott Laboratories, Lake County, IL, USA). Note, CG4+ measurements for TCO₂, sO₂, and BE in our perfusion media were either not detectable or irrelevant due to the removal of erythrocytes and continuous oxygenation of the media. Cotyledons were then biopsied for histological and molecular analyses.

Immunohistochemistry (IHC). 1 cm x 1 cm biopsies were placed in five times their volume of NBF (Thermo Fisher Scientific, Waltham, MA, USA). Samples fixed at 4 °C for a minimum of 7 days before processing and paraffin embedding. Sections were cut 4 μm thick, cleared and antigen retrieval for most targets was conducted at 110 °C for 15 min using the Decloaking Chamber NxGen (Biocare Medical, Pacheco, CA, USA). Only Ki67 staining's were conducted using a water bath heated to 95 °C for 15 min. All antigen retrievals were conducted with citrate buffer pH 6.0 (Vector labs, Burlingame, CA, USA) + 0.5% Tween 20 (Sigma). Blocking was conducted with the peroxide blocking kit (Dako-Agilent, Santa Clara, CA, USA) and then with Streptavidin-Biotin kit (Vector) according to manufacturer instructions, before sections were left overnight at 4 °C in PBS + 1% BSA containing 10% Donkey serum (Jackson Immuno Research, West Grove, PA, USA). The next day primary antibodies or isotype controls were applied in PBS + 1% BSA overnight at 4 °C. Staining was completed the following day with the RTU secondary kits (Vector) applied for 1 h and then administration of 3',3'-diaminobenzidine (DAB) (Vector) for up to 1 min. Terminal deoxynucleotidyl transferase dUTP nick end labeling (TUNEL) stainings were conducted with the TACS TdT-DAB In Situ Apoptosis Detection kit (R&D/Bio-Techne, Minneapolis, MN, USA) following manufacturer's instructions with the following key details: proteinase K was incubated for 15 min and TdT labeling was done with the cobalt cation for 5 min. All slides were counterstained with hematoxylin and coverslipped with a Tissue-Tek Prisma Plus with Film automated slide stainer (Sakura Finetek, Torrance, CA, USA).

Histological quantifications were conducted blinded using 40x images in ImageJ (NIH) for baseline, control and virus exposed samples from all ZIKV ($n = 10$) and iZIKV ($n = 9$) perfusion experiments. Images were acquired with a Leica SP8 system and DFC7000 camera (Buffalo Grove, IL, USA). A minimum of 3 images from each section/staining were analyzed to generate a mean value for each biological sample. For syncytium Injury, the amount of Placental Alkaline Phosphatase (PLAP) staining within regions of interest drawn over damaged areas was measured relative to the total area of PLAP staining per field. The total area of PLAP staining constitutes the proportion of PLAP pixels over tissue pixels, omitting the intervellous space to account for differences in the amount of syncytium between fields. TUNEL or Ki67 positive nuclei were counted using the ImageJ cell counter application. CD163 was measured as the percentage of DAB staining within each field. All histological counts/measurements were normalized to the area of placental tissue (omitting the maternal space) within each respective image.

Immunofluorescence (IF). A second 1 cm x 1 cm biopsy was fixed in 4% formaldehyde in PBS (made from powder, Sigma) for 2 h and left overnight in PBS + 30% Sucrose. Samples were embedded in OCT and frozen with 2-methylbutane cooled below -150 °C using LN2. Sections were cut 8 μm thick and blocked once more overnight with PBS + 1% BSA with 10% Donkey serum. Primary antibodies were again diluted in PBS + 1% BSA and left overnight at 4 °C. Secondary antibodies were also diluted in PBS + 1% BSA and applied for 1 h. DAPI (Thermo) was applied before coverslipping with ProLong Diamond mounting media (Thermo). Confocal images were acquired using a DMI8 TCS SPE II system (Leica) using the same parameters for controls and experimental samples. Antibodies details and dilutions for IHC and IF are listed in Supplementary Table 2.

Plaque assay. Vero cells were seeded into 12-well plates at 5×10^5 cells per well. After 24 h, monolayers were inoculated with 100 μl of 10-fold serial dilution of ZIKV or iZIKV stock in DMEM supplemented with 2% FBS and 1% Antibiotic Antimycotic. The plates were rocked every 15 mins for 1 h at 37 °C after which inoculum was removed and replaced with a 1% agar overlay. Four days later a second 1% agarose overlay containing 2% Neutral Red (Sigma-Aldrich) was added for 4 h at which point plaques became visible. After visual confirmation of plaques, plates were fixed in 10% neutral buffered formalin for 1 h. After fixation agar plugs were removed and the plates were stained with 1% crystal violet for 5 min. Crystal violet was then removed and plates were air dried and imaged.

RNA extraction. 0.5 cm x 0.5 cm biopsies were placed in individual tubes containing 4 ml ice-cold RNeasy Lysis Buffer (Thermo) and transferred to 4 °C. Within 7 days, samples were transferred from the RNeasy Lysis Buffer to empty tubes and placed at -80 °C for long-term storage. At the time of sample processing, tissues were weighed and homogenized in 1 ml Qiazol Reagent (QIAGEN, Valencia, CA, USA) using a bead-beater apparatus (Precellys, Bertin Corp., Rockville, MD, USA). Total RNA was isolated from 350 μl homogenate using a phenol-chloroform extraction method

and then purified with the RNeasy Lipid Tissue Mini Kit (QIAGEN, Valencia, CA, USA), in accordance with the manufacturer's instruction. RNA concentration was measured on the Qubit Fluorometer (Thermo) using the Qubit RNA Broad-Range Assay Kit (Thermo).

Viral load analysis. Viral RNA was measured in placenta tissue using a ZIKV prME-specific qRT-PCR assay. Three biopsies from each of the ten ZIKV exposed cotyledons were individually analyzed. A total of 400 ng of RNA was used to generate cDNA using the iScript Select cDNA Synthesis Kit (Bio-Rad, Hercules, CA, USA) following the manufacturer's protocol for gene-specific priming. Viral RNA copy number was quantified using the TaqMan Universal Master Mix containing AmpliTaq Gold DNA Polymerase (Thermo) on a ViiA7 Real-time PCR System instrument. ZIKV primers and probe were previously described and correspond to residues in the ZIKV F5513025 prME genomic region (GenBank no. MH368551) that are conserved in the ZIKV Brazil genome (GenBank no. KX811222). Standard dilutions and experimental cDNAs were run in triplicate. The standard curve was used to calculate the ZIKV copy number per μg of tissue. Samples with at least two of three replicates within the linear range of the standard curve were considered positive. To adhere to stringent guidelines, Ct (cycle threshold) values >38 were deemed as not reliably detected and were not reported. Baseline and control-perfused for the ten placenta donors were determined to be negative based on these criteria. Copy number sensitivity using a standard curve from serial dilutions of ZIKV genome was 25 copies/qRT-PCR reaction.

Gene expression analysis. The NanoString nCounter platform (NanoString, Seattle, WA, USA) as used to assess placenta gene expression in sixty tissue biopsies. Two biopsies per cotyledon were analyzed for each condition (Baseline, Control, ZIKV, and iZIKV) from $n = 5$ ZIKV and $n = 5$ iZIKV perfusion experiments. From each sample, 150 ng RNA was processed and loaded in accordance with manufacturer's instructions for targeted expression with the NanoString Human PanCancer Immunology Panel. Following the acquisition, we normalized gene expression values by estimating factors of unwanted variation with RUVg⁷⁹. This approach uses the NanoString panel of housekeeping genes to estimate factors of technical variation observed in the dataset⁷⁹. We selected one factor of unwanted variation to remove from the dataset and visualized RUVg normalized counts via principal component analysis and relative log expression plots, which resulted in the removal of a single outlier. Using the raw count matrix with the outliers removed, we performed trimmed mean of M-values normalization with edgeR and logCPM transformation with the voom function in limma⁸⁰⁻⁸³. The normalized count matrix was fit to a linear model with treatment included as the main effect and the RUVg factor of unwanted variation included as a covariate. Differential expression testing was performed in limma using a robust empirical Bayes moderation of the fitted linear model to control for hypo- & hyper-variable genes (e.g. sex-specific gene expression)⁸⁴. Paired differential expression contrasts were performed for each treatment group against their matched controls. A difference of differences contrast (i.e. interaction model) was also performed to compare the responses to iZIKV exposure and ZIKV infection while controlling for baseline differences. In each contrast, a gene was considered DE if the unadjusted p value < 0.05, as suggested by the NanoString Gene Expression Data Analysis Guidelines. The union of DE genes in at least one contrast were visualized in a heatmap using the R package pheatmap.

IFITM1 Quantitative Real-Time PCR. This analysis was conducted on the same samples examined with the NanoString nCounter platform. Coding DNAs were generated from 100 ng total RNA using random priming that followed the iScript[™] cDNA Synthesis Kit (Bio-Rad) instructions. The PCR was performed using the SYBR Green-Real-Time PCR Master Mix (Thermo) and with gene primer sets human *IFITM1* (Interferon Induced Transmembrane Protein 1) and human *RPL13A* (Ribosomal Protein L13a), previously reported⁵⁸. Plates were run on a ViiA 7 Real-Time PCR System with 384-well block (Thermo). Reactions for *hIFITM1* and *hRPL13A* were done in triplicate and the relative expression was calculated by the delta-delta Ct method.

Statistics and Reproducibility. Datasets for Figs. 1–8 and supplementary data 1 were analyzed using Excel (Microsoft, Redmond, WA, USA) and SPSS (IBM, Armonk, NY, USA). Quantitative comparisons were conducted with paired or unpaired student's t -test, as appropriate, and one-way ANOVA with Tukey's post hoc test. Categorical data was compared with chi-squared test. Experiments comparing ZIKV were reproduced across 10 placentas. For experiments involving iZIKV, 9 placentas were utilized.

Bioinformatics analysis. NanoString gene expression analysis was conducted in RStudio version 1.2.1335 with R version 4.0.0 using the following Bioconductor version 3.11 libraries: RUVSeq version 0.99.1, limma version 3.44.1, edgeR version 3.30.0, and EDASeq version 2.22.0⁸⁵. Functional analysis of gene expression datasets was performed using Ingenuity[®] Pathway Analysis (IPA, QIAGEN, Inc.)⁸⁶. The software tool analyzes the experimental dataset in the context of known biological functions and pathways within the Ingenuity Pathways Knowledge Base, a curated repository of biological interactions and functional annotations.

Canonical pathways analysis identifies IPA pathways that were significantly enriched ($p < 0.05$) and predicts the changes in pathways based on the observed expression changes of genes within each pathway. The p -value associated with each pathway was calculated using the right-tailed Fisher's exact test.

Figures. Graphs were generated using Excel, PowerPoint (Microsoft), and R. Figures were compiled using Photoshop (Adobe, San Jose, CA, USA). Brightness and contrast were adjusted as necessary to increase visibility; controls were adjusted equally to experimental samples. NanoString figures were generated with the R graphics package for volcano plots and heatmap (version 1.0.123) for co-expression heatmaps.

Reporting summary. Further information on research design is available in the Nature Research Reporting Summary linked to this article.

Data availability

The source data behind the graphs are available in Supplementary Data 2. All other data are available from the corresponding author on reasonable request and with institutional approval.

Received: 18 May 2021; Accepted: 9 February 2022;

Published online: 18 March 2022

References

- Petersen, L. R., Jamieson, D. J., Powers, A. M. & Honein, M. A. Zika Virus. *N. Engl. J. Med.* **374**, 1552–1563 (2016).
- Mead, P. S., Hills, S. L. & Brooks, J. T. Zika virus as a sexually transmitted pathogen. *Curr. Opin. Infect. Dis.* **31**, 39–44 (2018).
- Teixeira, F. M. E., Pietrobbon, A. J., Oliveira, L. M., Oliveira, L. & Sato, M. N. Maternal-Fetal Interplay in Zika Virus Infection and Adverse Perinatal Outcomes. *Front Immunol.* **11**, 175 (2020).
- Araujo, A. Q., Silva, M. T. & Araujo, A. P. Zika virus-associated neurological disorders: a review. *Brain: a J. Neurol.* **139**, 2122–2130 (2016).
- Depoux, A. et al. A multi-faceted pandemic: a review of the state of knowledge on the Zika virus. *Public Health Rev.* **39**, 10 (2018).
- Calvet, G. et al. Detection and sequencing of Zika virus from amniotic fluid of fetuses with microcephaly in Brazil: a case study. *Lancet Infect. Dis.* **16**, 653–660 (2016).
- Bhatnagar, J. et al. Zika Virus RNA Replication and Persistence in Brain and Placental Tissue. *Emerg. Infect. Dis.* **23**, 405–414 (2017).
- Adibi, J. J., Marques, E. T. A. Jr., Cartus, A. & Beigi, R. H. Teratogenic effects of the Zika virus and the role of the placenta. *Lancet* **387**, 1587–1590 (2016).
- Sheridan, M. A. et al. Vulnerability of primitive human placental trophoblast to Zika virus. *Proc. Natl Acad. Sci. USA* **114**, E1587–E1596 (2017).
- Hirsch, A. J. et al. Zika virus infection in pregnant rhesus macaques causes placental dysfunction and immunopathology. *Nat. Commun.* **9**, 263 (2018).
- Adams Waldorf, K. M. et al. Fetal brain lesions after subcutaneous inoculation of Zika virus in a pregnant nonhuman primate. *Nat. Med.* **22**, 1256–1259 (2016).
- Adams Waldorf, K. M. et al. Congenital Zika virus infection as a silent pathology with loss of neurogenic output in the fetal brain. *Nat. Med.* **24**, 368–374 (2018).
- Caine, E. A., Jagger, B. W. & Diamond, M. S. Animal Models of Zika Virus Infection during Pregnancy. *Viruses* **10**, 110598 (2018).
- Grigsby, P. L. Animal Models to Study Placental Development and Function throughout Normal and Dysfunctional Human Pregnancy. *Semin Reprod. Med.* **34**, 11–16 (2016).
- Honein, M. A. et al. Birth Defects Among Fetuses and Infants of US Women With Evidence of Possible Zika Virus Infection During Pregnancy. *JAMA* **317**, 59–68 (2017).
- Reynolds, M. R. et al. Vital Signs: Update on Zika Virus-Associated Birth Defects and Evaluation of All U.S. Infants with Congenital Zika Virus Exposure - U.S. Zika Pregnancy Registry, 2016. *MMWR Morb. Mortal. Wkly Rep.* **66**, 366–373 (2017).
- Shapiro-Mendoza, C. K. et al. Pregnancy Outcomes After Maternal Zika Virus Infection During Pregnancy - U.S. Territories, January 1, 2016–April 25, 2017. *MMWR Morb. Mortal. Wkly Rep.* **66**, 615–621 (2017).
- Venceslau, E. M. et al. Adequate Placental Sampling for the Diagnosis and Characterization of Placental Infection by Zika Virus. *Front Microbiol* **11**, 112 (2020).
- Duffy, M. R. et al. Zika virus outbreak on Yap Island, Federated States of Micronesia. *N. Engl. J. Med.* **360**, 2536–2543 (2009).
- Reagan-Steiner, S. et al. Evaluation of Placental and Fetal Tissue Specimens for Zika Virus Infection - 50 States and District of Columbia, January–December, 2016. *MMWR Morb. Mortal. Wkly Rep.* **66**, 636–643 (2017).
- Robbiani, D. F. et al. Risk of Zika microcephaly correlates with features of maternal antibodies. *J. Exp. Med.* **216**, 2302–2315 (2019).
- Reed, L. C., Estrada, S. M., Walton, R. B., Napolitano, P. G. & Ieronimakis, N. Evaluating maternal hyperglycemic exposure and fetal placental arterial dysfunction in a dual cotyledon, dual perfusion model. *Placenta* **69**, 109–116 (2018).
- Walton, R. B. et al. Evaluation of Sildenafil and Tadalafil for Reversing Constriction of Fetal Arteries in a Human Placenta Perfusion Model. *Hypertension* **72**, 167–176 (2018).
- Lee, K. J. et al. Global gene expression changes induced in the human placenta during labor. *Placenta* **31**, 698–704 (2010).
- de Noronha, L. et al. Zika Virus Infection at Different Pregnancy Stages: Anatomopathological Findings, Target Cells and Viral Persistence in Placental Tissues. *Front Microbiol* **9**, 2266 (2018).
- Cannell, G. R. et al. Markers of physical integrity and metabolic viability of the perfused human placental lobule. *Clin. Exp. Pharm. Physiol.* **15**, 837–844 (1988).
- Loegl, J. et al. Hofbauer cells of M2a, M2b and M2c polarization may regulate fetal-placental angiogenesis. *Reproduction* **152**, 447–455 (2016).
- Muhlhauser, J., Crescimanno, C., Kasper, M., Zaccheo, D. & Castellucci, M. Differentiation of human trophoblast populations involves alterations in cytokeratin patterns. *J. Histochem Cytochem* **43**, 579–589 (1995).
- Redman, C. W. & Sargent, I. L. Circulating microparticles in normal pregnancy and pre-eclampsia. *Placenta* **29**, S73–S77 (2008). **Suppl. A**.
- Etzerodt, A. & Moestrup, S. K. CD163 and inflammation: biological, diagnostic, and therapeutic aspects. *Antioxid. Redox Signal* **18**, 2352–2363 (2013).
- Gavrieli, Y., Sherman, Y. & Ben-Sasson, S. A. Identification of programmed cell death in situ via specific labeling of nuclear DNA fragmentation. *J. Cell Biol.* **119**, 493–501 (1992).
- Gerdes, J. et al. Cell cycle analysis of a cell proliferation-associated human nuclear antigen defined by the monoclonal antibody Ki-67. *J. Immunol.* **133**, 1710–1715 (1984).
- Foo, S. S. et al. Asian Zika virus strains target CD14(+) blood monocytes and induce M2-skewed immunosuppression during pregnancy. *Nat. Microbiol* **2**, 1558–1570 (2017).
- Tabata, T. et al. Zika Virus Targets Different Primary Human Placental Cells, Suggesting Two Routes for Vertical Transmission. *Cell Host Microbe* **20**, 155–166 (2016).
- Esteves, E., Rosa, N., Correia, M. J., Arrais, J. P. & Barros, M. New Targets for Zika Virus Determined by Human-Viral Interactomic: A Bioinformatics Approach. *Biomed. Res Int* **2017**, 1734151 (2017).
- Ojha, C. R. et al. Toll-like receptor 3 regulates Zika virus infection and associated host inflammatory response in primary human astrocytes. *PLoS One* **14**, e0208543 (2019).
- Mittal, P. et al. CXCL6 (granulocyte chemotactic protein-2): a novel chemokine involved in the innate immune response of the amniotic cavity. *Am. J. Reprod. Immunol.* **60**, 246–257 (2008).
- Wang, Q. et al. Soluble interleukin-6 receptor-mediated innate immune response to DNA and RNA viruses. *J. Virol.* **87**, 11244–11254 (2013).
- Yang, H. L. et al. Decidual stromal cells maintain decidual macrophage homeostasis by secreting IL-24 in early pregnancy. *Am. J. Reprod. Immunol.* **84**, e13261 (2020).
- Taglauer, E. S., Trikhacheva, A. S., Slusser, J. G. & Petroff, M. G. Expression and function of PDCD1 at the human maternal-fetal interface. *Biol. Reprod.* **79**, 562–569 (2008).
- Moroi, H. et al. The expression of Toll-like receptor 5 in preterm histologic chorioamnionitis. *J. Clin. Biochem Nutr.* **62**, 63–67 (2018).
- Roby, J. A. et al. Flavivirus Nonstructural Protein NS5 Dysregulates HSP90 to Broadly Inhibit JAK/STAT Signaling. *Cells* **9**, 899 (2020).
- Haby, M. M., Pinart, M., Elias, V. & Reveiz, L. Prevalence of asymptomatic Zika virus infection: a systematic review. *Bull. World Health Organ* **96**, 402–413D (2018).
- Halai, U. A. et al. Maternal Zika Virus Disease Severity, Virus Load, Prior Dengue Antibodies, and Their Relationship to Birth Outcomes. *Clin. Infect. Dis.* **65**, 877–883 (2017).
- Foo, S. S. et al. Biomarkers and immunoprofiles associated with fetal abnormalities of ZIKV-positive pregnancies. *JCI Insight* **3**, e124152 (2018).
- Scott, J. M. et al. Cellular and Humoral Immunity Protect against Vaginal Zika Virus Infection in Mice. *J. Virol.* **92**, e00038–18 (2018).
- Caires-Junior, L. C. et al. Publisher Correction: Discordant congenital Zika syndrome twins show differential in vitro viral susceptibility of neural progenitor cells. *Nat. Commun.* **9**, 1114 (2018).
- Schumacher, A., Sharkey, D. J., Robertson, S. A. & Zenclussen, A. C. Immune Cells at the Fetomaternal Interface: How the Microenvironment Modulates Immune Cells To Foster Fetal Development. *J. Immunol.* **201**, 325–334 (2018).
- Kourtis, A. P., Read, J. S. & Jamieson, D. J. Pregnancy and infection. *N. Engl. J. Med.* **370**, 2211–2218 (2014).

50. Jauniaux, E. et al. Materno-fetal immunoglobulin transfer and passive immunity during the first trimester of human pregnancy. *Hum. Reprod.* **10**, 3297–3300 (1995).
51. Ciobanu, A. M. et al. Benefits and Risks of IgG Transplacental Transfer. *Diagnostics (Basel)* **10**, <https://doi.org/10.3390/diagnostics10080583> (2020).
52. Grant, A. et al. Zika Virus Targets Human STAT2 to Inhibit Type I Interferon Signaling. *Cell Host Microbe* **19**, 882–890 (2016).
53. Jurado, K. A. et al. Zika virus productively infects primary human placenta-specific macrophages. *JCI Insight* **1**, e88461 (2016).
54. Vermillion, M. S. et al. Intrauterine Zika virus infection of pregnant immunocompetent mice models transplacental transmission and adverse perinatal outcomes. *Nat. Commun.* **8**, 14575 (2017).
55. Miranda, J. et al. Syncytiotrophoblast of Placentae from Women with Zika Virus Infection Has Altered Tight Junction Protein Expression and Increased Paracellular Permeability. *Cells* **8**, 1174 (2019).
56. Quicke, K. M. et al. Zika Virus Infects Human Placental Macrophages. *Cell Host Microbe* **20**, 83–90 (2016).
57. Kumar, A. et al. Zika virus inhibits type-I interferon production and downstream signaling. *EMBO Rep.* **17**, 1766–1775 (2016).
58. Esser-Nobis, K. et al. Comparative Analysis of African and Asian Lineage-Derived Zika Virus Strains Reveals Differences in Activation of and Sensitivity to Antiviral Innate Immunity. *J. Virol.* **93**, e00640–19 (2019).
59. Schwartz, D. A. Viral infection, proliferation, and hyperplasia of Hofbauer cells and absence of inflammation characterize the placental pathology of fetuses with congenital Zika virus infection. *Arch. Gynecol. Obstet.* **295**, 1361–1368 (2017).
60. Yockey, L. J. et al. Type I interferons instigate fetal demise after Zika virus infection. *Sci. Immunol.* **3**, aao1680 (2018).
61. Rabelo, K. et al. Zika Induces Human Placental Damage and Inflammation. *Front Immunol.* **11**, 2146 (2020).
62. Chen, J. et al. Outcomes of Congenital Zika Disease Depend on Timing of Infection and Maternal-Fetal Interferon Action. *Cell Rep.* **21**, 1588–1599 (2017).
63. Silen, M. L., Firpo, A., Morgello, S., Lowry, S. F. & Francus, T. Interleukin-1 alpha and tumor necrosis factor alpha cause placental injury in the rat. *Am. J. Pathol.* **135**, 239–244 (1989).
64. Brasil, P. et al. Zika Virus Infection in Pregnant Women in Rio de Janeiro. *N. Engl. J. Med.* **375**, 2321–2334 (2016).
65. Guller, S. Role of the syncytium in placenta-mediated complications of preeclampsia. *Thromb. Res* **124**, 389–392 (2009).
66. Pineda, A., Verdín-Teran, S. L., Camacho, A. & Moreno-Fierros, L. Expression of toll-like receptor TLR-2, TLR-3, TLR-4 and TLR-9 is increased in placentas from patients with preeclampsia. *Arch. Med Res* **42**, 382–391 (2011).
67. Holcberg, G. et al. Increased production of tumor necrosis factor-alpha TNF-alpha by IUGR human placenta. *Eur. J. Obstet. Gynecol. Reprod. Biol.* **94**, 69–72 (2001).
68. Almasry, S. M., Eldomiaty, M. A., Elfayomy, A. K. & Habib, F. A. Expression pattern of tumor necrosis factor alpha in placenta of idiopathic fetal growth restriction. *J. Mol. Histol.* **43**, 253–261 (2012).
69. Hu, Y. et al. Zika virus antagonizes interferon response in patients and disrupts RIG-I-MAVS interaction through its CARD-TM domains. *Cell Biosci.* **9**, 46 (2019).
70. Carlin, A. F. et al. Deconvolution of pro- and antiviral genomic responses in Zika virus-infected and bystander macrophages. *Proc. Natl Acad. Sci. USA* **115**, E9172–E9181 (2018).
71. Patterson, B. K. et al. Leukemia inhibitory factor inhibits HIV-1 replication and is upregulated in placenta from nontransmitting women. *J. Clin. Invest* **107**, 287–294 (2001).
72. Bowers, J. R., Readler, J. M., Sharma, P. & Excoffon, K. Poliovirus Receptor: More than a simple viral receptor. *Virus Res* **242**, 1–6 (2017).
73. Human Protein Atlas available from <http://www.proteinatlas.org>.
74. Belizario, J. E., Neyra, J. M. & Setubal Destro Rodrigues, M. F. When and how NK cell-induced programmed cell death benefits immunological protection against intracellular pathogen infection. *Innate Immun.* **24**, 452–465 (2018).
75. Nguyen, S. M. et al. Highly efficient maternal-fetal Zika virus transmission in pregnant rhesus macaques. *PLoS Pathog.* **13**, e1006378 (2017).
76. Rodo, C. et al. Pregnancy outcomes after maternal Zika virus infection in a non-endemic region: prospective cohort study. *Clin. Microbiol Infect.* **25**, 633 e635–633 e639 (2019).
77. Nogueira, M. L. et al. Adverse birth outcomes associated with Zika virus exposure during pregnancy in Sao Jose do Rio Preto, Brazil. *Clin. Microbiol Infect.* **24**, 646–652 (2018).
78. Noronha, L., Zanluca, C., Azevedo, M. L., Luz, K. G. & Santos, C. N. Zika virus damages the human placental barrier and presents marked fetal neurotropism. *Mem. Inst. Oswaldo Cruz* **111**, 287–293 (2016).
79. Risso, D., Ngai, J., Speed, T. P. & Dudoit, S. Normalization of RNA-seq data using factor analysis of control genes or samples. *Nat. Biotechnol.* **32**, 896–902 (2014).
80. McCarthy, D. J., Chen, Y. & Smyth, G. K. Differential expression analysis of multifactor RNA-Seq experiments with respect to biological variation. *Nucleic Acids Res* **40**, 4288–4297 (2012).
81. Robinson, M. D., McCarthy, D. J. & Smyth, G. K. edgeR: a Bioconductor package for differential expression analysis of digital gene expression data. *Bioinformatics* **26**, 139–140 (2010).
82. Law, C. W., Chen, Y., Shi, W. & Smyth, G. K. voom: Precision weights unlock linear model analysis tools for RNA-seq read counts. *Genome Biol.* **15**, R29 (2014).
83. Ritchie, M. E. et al. limma powers differential expression analyses for RNA-sequencing and microarray studies. *Nucleic Acids Res.* **43**, e47 (2015).
84. Phipson, B., Lee, S., Majewski, I. J., Alexander, W. S. & Smyth, G. K. Robust Hyperparameter Estimation Protects against Hypervariable Genes and Improves Power to Detect Differential Expression. *Ann. Appl. Stat.* **10**, 946–963 (2016).
85. Huber, W. et al. Orchestrating high-throughput genomic analysis with Bioconductor. *Nat. Methods* **12**, 115–121 (2015).
86. Kramer, A., Green, J., Pollard, J. Jr. & Tugendreich, S. Causal analysis approaches in Ingenuity Pathway Analysis. *Bioinformatics* **30**, 523–530 (2014).

Acknowledgements

We are grateful for funding from the Department of Clinical Investigations, Madigan Army Medical Center and philanthropic support to the UW Center for Innate Immunity and Immune Disease and from the National Institute of Health (NIH) grants AI145296, AI143265, and OD010425. The views expressed are those of the author(s) and do not reflect the official policy of the Department of the Army, the Department of Defense or the U.S.

Author contributions

D.L.V., K.M.W., P.G.N., J.T.-G., N.I., and M.G. planned the study. D.L.V., K.M.W., J.R.D., E.M.D., J.A.P., K.V., A.M., S.S.S., S.M.M., A.M., J.T.-G., and N.I. worked out technical details, conducted experiments and data analyses. D.L.V., K.M.W., D.N., P.G.N., J.T.-G., N.I., and M.G. drafted and edited the manuscript.

Competing interests

The authors declare no competing interests.

Ethical approval

The investigators have adhered to the policies for the protection of human subjects as prescribed in 45 CFR 46.

Additional information

Supplementary information The online version contains supplementary material available at <https://doi.org/10.1038/s42003-022-03158-6>.

Correspondence and requests for materials should be addressed to Nicholas Ieronimakis or Michael Gale Jr.

Peer review information *Communications Biology* thanks Suan-Sin Foo and the other, anonymous, reviewer(s) for their contribution to the peer review of this work. Primary Handling Editors Christina Karlsson Rosenthal.

Reprints and permission information is available at <http://www.nature.com/reprints>

Publisher's note Springer Nature remains neutral with regard to jurisdictional claims in published maps and institutional affiliations.



Open Access This article is licensed under a Creative Commons Attribution 4.0 International License, which permits use, sharing, adaptation, distribution and reproduction in any medium or format, as long as you give appropriate credit to the original author(s) and the source, provide a link to the Creative Commons license, and indicate if changes were made. The images or other third party material in this article are included in the article's Creative Commons license, unless indicated otherwise in a credit line to the material. If material is not included in the article's Creative Commons license and your intended use is not permitted by statutory regulation or exceeds the permitted use, you will need to obtain permission directly from the copyright holder. To view a copy of this license, visit <http://creativecommons.org/licenses/by/4.0/>.

This is a U.S. government work and not under copyright protection in the U.S.; foreign copyright protection may apply 2022